microbial biotechnology

Open Access

Comprehensively dissecting the hub regulation of PkaC on high-productivity and pellet macromorphology in citric acid producing *Aspergillus niger*

Xiaomei Zheng,[1,2,3,4] Timothy C. Cairns,[1,2,5] Xiaomei Ni,[1,2,4] Lihui Zhang,[1,2,4] Huanhuan Zhai,[1] Vera Meyer,[5] Ping Zheng[1,2,3,4] and Jibin Sun[1,2,3,4]

[1]*Tianjin Institute of Industrial Biotechnology, Chinese Academy of Sciences, 32 West 7th Avenue, Tianjin, 300308, China.*

[2]*Key Laboratory of Systems Microbial Biotechnology, Chinese Academy of Sciences, Tianjin, 300308, China.*

[3]*University of Chinese Academy of Sciences, Beijing, 100049, China.*

[4]*National Technology Innovation Center of Synthetic Biology, Tianjin, 300308, China.*

[5]*Institute of Biotechnology, Chair of Applied and Molecular Microbiology, Technische Universität Berlin, Berlin, 13355, Germany.*

Summary

***Aspergillus niger*, an important industrial workhorse for citric acid production, is characterized by polar hyphal growth with complex pelleted, clumped or dispersed macromorphologies in submerged culture. Although organic acid titres are dramatically impacted by these growth types, studies that assess productivity and macromorphological changes are limited. Herein, we functionally analysed the role of the protein kinase A (PKA)/cyclic adenosine monophosphate (cAMP) signalling cascade during fermentation by disrupting and conditionally expressing the *pkaC* gene. *pkaC* played multiple roles during hyphal, colony and conidiophore growth. By overexpressing *pkaC*, we could concomitantly modify hyphal growth at the pellet surface and improve citric acid titres up to 1.87-fold. By quantitatively analysing hundreds of pellets during pilot fermentation experiments, we provide the first comprehensive correlation between *A. niger* pellet surface morphology and citric acid production. Finally, by intracellular metabolomics analysis and weighted gene coexpression network analysis (WGCNA) following titration of *pkaC* expression, we unveil the metabolomic and transcriptomic basis underpin hyperproductivity and pellet growth. Taken together, this study confirms *pkaC* as hub regulator linking submerged macromorphology and citric acid production and provides high-priority genetic leads for future strain engineering programmes.**

Received 10 October, 2021; revised 20 January, 2022; accepted 8 February, 2022.

For correspondence. *E-mail zheng_p@tib.cas.cn; Tel. +86-22-84861945; Fax +86-22-84861943. **E-mail sun_jb@tib.cas.cn; Tel. +86-22-84861949; Fax +86-22-84861943.

Microbial Biotechnology (2022) **15**(6), 1867–1882
doi:10.1111/1751-7915.14020

Funding information

This study was supported by the National Key R&D Programme of China (2018YFA0900500), National Natural Sciences Foundation of China (31961133021 and 32070082), Tianjin Synthetic Biotechnology Innovation Capacity Improvement Project (TSBICIP-PTJS-003), Deutsche Forschungs gemeinschaft (DFG) for the financial support for this work grant ME 2041/13-1.

Introduction

Citric acid, a well-known intermediate of the tricarboxylic acid cycle (TCA), is the most important bulk industrial organic acid product with the worldwide market of nearly 2 million tons per year (Tong *et al.*, 2019). Citric acid has been widely applied in beverage and food, pharmaceutical, detergents, cosmetics and organic chemical industries for over a century (Karaffa and Kubicek, 2003; Legisa and Mattey, 2007; Cairns *et al.*, 2018; Tong *et al.*, 2019). Due to high production capacity, robust stress tolerance and the ability to utilize a wide range of carbon sources, *Aspergillus niger* is widely exploited as an industrial workhorse for the citric acid production. Approximately 80% of worldwide citric acid is produced by submerged fermentation using *A. niger* (Dhillon *et al.*, 2011).

As a filamentous fungus, *A. niger* growth is characterized by germination of metabolically dormant spores and extension/branching of highly polar cells termed hyphae (Meyer *et al.*, 2021). Depending on the *A. niger* strain and culture conditions during submerged fermentation, different macromorphologies are formed, varying from freely dispersed mycelium, loose mycelial clumps, pellets of various sizes and densities, or heterogeneous mixes of these growth types (Papagianni, 2004; Casas Lopez *et al.*, 2005; Cairns *et al.*, 2019a). Various morphologies of filamentous fungi play vital roles for productivity, owing to their important influence on the Newtonian flow

behaviour of culture broth and gas/liquid mass transfer of oxygen during the industrial fermentation process (Papagianni and Mattey, 2006). Importantly, mycelial pellets enhance sheer stress resistance and reduce the fermentation broth viscosity, which is proven to be more suitable to citric acid production (Gomez *et al.*, 1988; Papagianni, 2004). Although these studies described morphological changes and optimization in qualitative or semi-quantitative terms, the awareness of more precise morphological parameters of optimal pellets for citric acid production (e.g. diameter, aspect ratio, surface structure) is still vague.

Many efforts have been taken to control fungal growth and morphology during industrial bioprocesses by modification of culture conditions including inoculum spore concentration (e.g. Papagianni and Mattey, 2006; Liu *et al.*, 2008; Bizukojc and Ledakowicz, 2010)), pH value and pH shifting (e.g. Bizukojc and Ledakowicz, 2009; Papagianni, 2004), cultivation temperature (e.g. Liu *et al.*, 2008) or medium composition (e.g. Henzler, 2000; Liu *et al.*, 2008; Papagianni and Mattey, 2004; Znidarsic *et al.*, 2000). Moreover, chassis strains have also been generated by engineering various genes to adjust the morphology, including the putative amino acid transporter Brsa-25 (Dai *et al.*, 2004), chitin synthase ChsC (Sun *et al.*, 2018) and a predicted component of the endosome cargo trafficking system ApID (Cairns *et al.*, 2019b). However, the number of gene candidates for generating morphologically optimized chassis strains with elevated citric acid titres is currently limited as the molecular basis between optimal morphology and hyperproductivity of citric acid has not been fully understood.

Recently, generation and mining of transcriptional coexpression networks have emerged as a powerful tool for generating high-priority candidate genes for engineering *A. niger* strains with optimal morphologies and/or elevated protein, organic acid and secondary metabolite titres (Schape *et al.*, 2019). This approach is based on the so-called guilt by association hypothesis, whereby genes involved in similar processes or pathways (e.g. productivity and morphology) are robustly coexpressed under different conditions. Consequently, candidate genes can be selected in a rational manner and tested individually or in combination to dissect their role in macromorphological development and productivity. It should be noted, however, that current publicly available coexpression resources were generated from over 280 microarray experiments covering a diverse compendium of strain and cultivation conditions. It is possible that a dedicated coexpression network generated from submerged cultivation with various macromorphologies and product titres will deliver a transcriptional network highly enriched for biotechnologically relevant coexpression relationships.

Since cell signalling, such as protein kinase A (PKA)/-cyclic adenosine monophosphate (cAMP) signalling cascade, plays an essential role in filamentous growth, key components of signalling cascades and their coexpressed genes could represent promising targets for morphology engineering and improved biotechnological applications (Brown *et al.*, 2015; Cairns *et al.*, 2019c; Choi *et al.*, 2020). Especially, the cAMP-dependent protein kinase (PKA), consisting of a regulatory subunit (PkaR) and a catalytic subunit (PkaC), is crucial for asexual development, carbon sensing and hyphal growth in *Aspergilli* spp (Saudohar *et al.*, 2002; Grosse *et al.*, 2008; de Assis *et al.*, 2015). For instance, Saudohar *et al* reported that absence of PKA activity led to very small colonies on plates and growth polarity loss during submerged growth in *A. niger* (Saudohar *et al.*, 2002), which suggested an essential effect of the PKA activity on mycelia morphogenesis. To comprehensively dissect its role in the regulation of morphology during citric acid fermentation, the *pkaC* gene, encoding the catalytic subunit of PKA, was chosen as the target in this study.

Here, we firstly demonstrate that the *pkaC* gene can be targeted to optimize submerged pellet macromorphology and elevate citric acid titres in *A. niger*. It demonstrated that the overexpression of *pkaC* enables to modify pellet surface structure and increase citric acid production about 1.87-fold compared to the reference strain, which strongly suggests modifications to pellet surface structure enables optimal citric acid productivity. Furthermore, RNA-seq and metabolomic profiling were conducted under the condition of titratable *pkaC* expression levels to underpin the *pkaC* regulation network using the weighted gene coexpression network analysis (WGCNA) approach, which enables identification of highly connected 'hub' genes, and the delineation of coexpression modules which are specifically associated with macromorphological development or citric acid productivity. These findings deepen the understanding on the regulation of pellet morphology and citric acid production and provide a basis for the further *A. niger* cell factory optimization.

Results

pkaC *is required for normal hyphal morphology, conidiophore development and colony growth in* A. niger

To dissect the effect of the PKA/cAMP signalling cascade on citric acid fermentation, we constructed *pkaC* deficient mutants and conditional expression mutants via the CRISPR/Cas9 system (Zheng *et al.*, 2019b) in citric acid producing *A. niger* isolate D353. In order to disrupt the gene *pkaC*, the hygromycin-resistant *hph* cassette was inserted into double-strand break (DSB) in the *pkaC* open reading frame following Cas9 nuclease activity to

generate mutant XMD3.5 (Fig. S1). For the *pkaC* conditional expression mutants, the titratable Tet-on cassette (Wanka *et al*., 2016) was inserted in the upstream of *pkaC* or replaced the *pkaC* promoter to generate mutants XMD4.1 and XMD5.1 respectively (Fig. S1). The Tet-on cassette is able to be titratably induced by addition of tetracycline derivative doxycycline (Dox), which facilitates the correlation between gene expression level and phenotype in a single mutant (Meyer *et al*., 2011a; Wanka *et al*., 2016).

In order to determine the influence of *pkaC* on *A. niger* hyphal, conidiophore and colony growth, phenotypic screens of the conditional expression mutants were conducted on growth media supplemented with 0, 0.2, 2 and 20 μg ml^{-1} Dox in order to model null, low, intermediate and overexpression respectively. All isolates were compared to the progenitor strain as control. Additionally, the *pkaC*-disrupted mutant XMD3.5 served as an additional control for the absence of gene expression in conditional expression mutants when grown under 0 μg ml^{-1} Dox. Without the addition of inducer Dox, colony growth on solid media of conditional expression mutants XMD4.1 and XMD5.1 was similar with the ones of XMD3.5, revealing compact colonies, which displayed reduced sporulation, thus confirming the *pkaC* gene plays an important role in colony growth and development (Fig. S1). The colony growth defects were titratable, as supplementation of 20 μg ml^{-1} Dox to growth media revealed XMD4.1 and XMD5.1 colony growth became broadly comparable to that of wild type (Fig. S1).

To unveil the effect of *pkaC* expression on conidiophore generation, conidiophore development was observed by SEM after cultivation on CM agar supplemented with 0, 2 and 20 μg ml^{-1} Dox. As shown in Fig. 1A, the conidiophores of *pkaC* disrupted mutant XMD3.5 were dramatically altered, which is similar to the conditional expressed mutants without addition of the inducer Dox (Fig. 1A). In addition, we also observed that *pkaC* disruption and its reduced expression resulted in curled aerial hypha and less spores (Fig. 1A). Moreover, under low Dox concentration, the conidiophore of the *pkaC* conditional expressed mutant generated more branches, which further grew into new conidiophores, bearing some conidia (Fig. S2). Similar to the phenotype of cell growth, with the increase of the inducer Dox, the conidiophore morphology of the *pkaC* was titratable. With 20 μg ml^{-1} Dox supplementation, the conidiophore of XMD4.1 and XMD5.1 resembled to the progenitor strain (Fig. 1A). It should be noted that conidial size and morphology of all detected strains did not show significant differences (Fig. S3). Taken together, *pkaC* expression is important for conidiophore development in *A. niger*.

Finally, to test the impact of *pkaC* expression levels on *A. niger* hyphal development, all strains were incubated at 30°C for 10 h in liquid MM supplemented with various Dox concentrations. Polarity establishment and branching frequencies were affected by *pkaC* expression (Fig. 1B). Without Dox addition, XM4.1 and XM5.1 showed similar hyphal morphological phenotypes with the *pkaC* disrupted mutant XM 3.5, with up to 2-3 branching points, while hyphal branches increased compared to the reference isolate (Fig. 1B). Titration of *pkaC* gene expression in isolate XM4.1 and XM5.1 using 20 μg ml^{-1} Dox resulted branching frequencies comparable to that of the progenitor strain (Fig. 1B). As to the hyphal length and hyphal diameter, there was no significant difference, except when 20 μg ml^{-1} Dox was supplemented (Fig. 1B). Taken together, these data confirm that the *pkaC* gene, and the PKA/cAMP signalling cascade, is important for polarity establishment/maintenance of young hyphae, colony growth and conidiophore development in *A. niger*. In the light of these data, we assumed that the *pkaC* mutants would display altered macromorphological development in submerged culture, which may elevate product titres.

pkaC *mutants display altered pellet macromorphologies when grown in submerged media*

In order to assess the role of *pkaC* expression on submerged culture, *pkaC* conditional expression mutants and the progenitor control were cultured in liquid citrate fermentation medium conventionally used to achieve high citrate production (CitFM medium, 12% total sugar, 34°C, pH 5.0). Cultivation medium was supplemented with 0, 0.2, 2, 20 or 50 μg ml^{-1} Dox. Representative images of pellet morphology in shake flask cultivations are shown in Fig. 2. Additionally, pellet Euclidian parameters (maximum diameter, area, solidity and aspect ratio, see methods) were quantified using the automated MPD image analysis pipeline (Cairns *et al*., 2019b) and used to determine the dimensionless morphology number (MN) (Wucherpfennig *et al*., 2011), which generates a value between 0 (a theoretical one-dimensional line) and 1 (a perfect round sphere).

Under all conditions, the wild-type control produced approximately spherical pellets 800 μm in diameter, with an average pellet solidity and MN of 0.82 and 0.62 respectively (Fig. 2). For the *pkaC* conditional expression strains XMD4.1 and XMD5.1, titratable expression of *pkaC* showed a close correlation with several macromorphological traits, but there was no distinguishable difference between the morphology of these two strains. With addition of 0 and 0.2 μg ml^{-1} Dox, the pellet size of XMD5.1 was significantly decreased, since the pellets have the less hypha at the pellet surface, resulting in

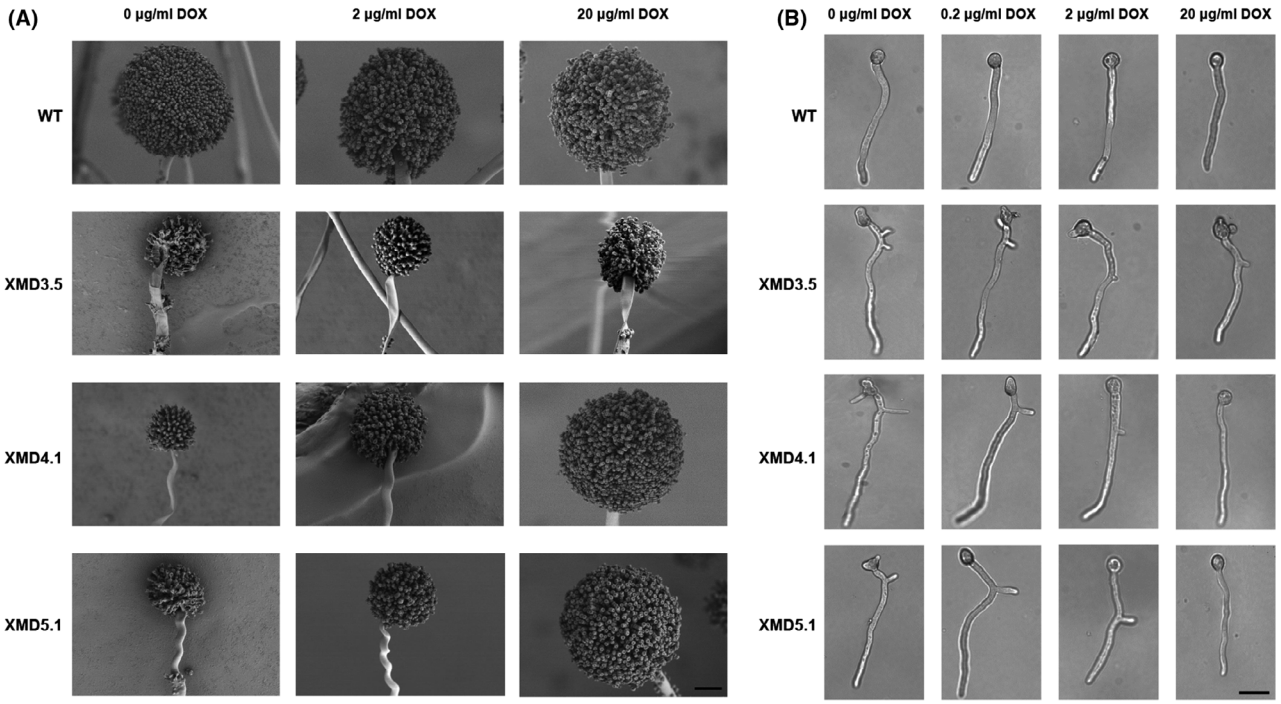

Fig. 1. *pkaC* impacts *A. niger* conidiophore development and hyphal morphology.
A. SEM microscopy of conidiophores at 96 h. All strains were streaked onto CM agar supplemented with various concentrations of Dox and then incubated at 30°C in the dark. Conidiophores of the corresponding cultures isolated using adhesive tape and then coated with gold and observed by SEM. Representative images were shown for technically triplicated experiments.
B. Hypha morphological characteristics of *pkaC* conditional expression mutants. 1×10^4 spores ml^{-1} were inoculated in 5 ml liquid MM media supplemented with various concentrations of Dox and were incubated at 30°C in the dark for 10 h. Representative images are shown for technically triplicated experiments. Scale bar depicts 10 μm. WT, progenitor strain; XMD3.5, the pkaC disrupted mutant; XMD4.1 and XMD5.1, pkaC conditional expression mutants.

higher solidity of 0.91 and 0.92 and significantly higher MN of 0.68 and 0.74 respectively (Fig. 2). When the Dox concentration increased up to 2 μg ml^{-1}, the pellet morphology of the *pkaC* conditional expression mutants resembled the control, with the solidity of 0.84 (Fig. 2). With the inducer of 20 μg ml^{-1} Dox, the overexpression of *pkaC* resulted in more significant pellet morphological changes, with the decreased solidity of 0.74 and MN of 0.55 respectively (Fig. 2). With 50 μg ml^{-1} Dox, the solidity and MN of XM5.1 reduced to 0.71 and 0.52 respectively (Fig. 2). Taken together, we conclude that *pkaC* plays an essential role in macromorphological development during submerged growth, and *pkaC* expression level is directly related to the pellet surface structure.

Overexpression of pkaC *increases intracellular and secreted citric acid titres in* A. niger

In order to determine the impact of *pkaC* expression levels on citric acid production, we conducted citric acid fermentation with various Dox concentrations using *pkaC* conditional expression mutants. The extracellular acid profiling was measured by HPLC (Fig. 3), and the intracellular metabolites involved in the central metabolism were determined by LC-MS/MS (Fig. 4). *pkaC* expression significantly influenced secreted citric acid titres, with null/lowered expression significantly reducing extracellular concentrations and overexpression causing a marked increase (Fig. 3). With 20 μg ml^{-1} Dox supplemented, the citric acid production of *pkaC* conditional expressed mutants XMD4.1 and XMD5.1 increased about 1.31-fold (29.67 ± 1.33 g l^{-1}) and 1.25-fold (28.29 ± 0.87 g l^{-1}) as that of the progenitor control (22.58 ± 2.11 g l^{-1}) respectively. Moreover, when 50 μg ml^{-1} Dox was supplemented, the citric acid production of XMD4.1 and XMD5.1 reached up to 1.83-fold (34.33 ± 0.47 g l^{-1}) and 1.87-fold (34.96 ± 1.05 g l^{-1}), respectively, compared to the wild-type control (18.73 ± 1.71 g l^{-1}) (Fig. 3). These data were supported by intracellular metabolomic analysis, which demonstrated increased titres of citric acid in the overexpression mutants compared to lowered *pkaC* expression and the progenitor control strain (Fig. 4).

Next, we quantitatively determined the correlation between the pellet morphological parameters and citric acid production (Fig. 3) by plotting pellet solidity of all test cultivations under various concentrations of Dox

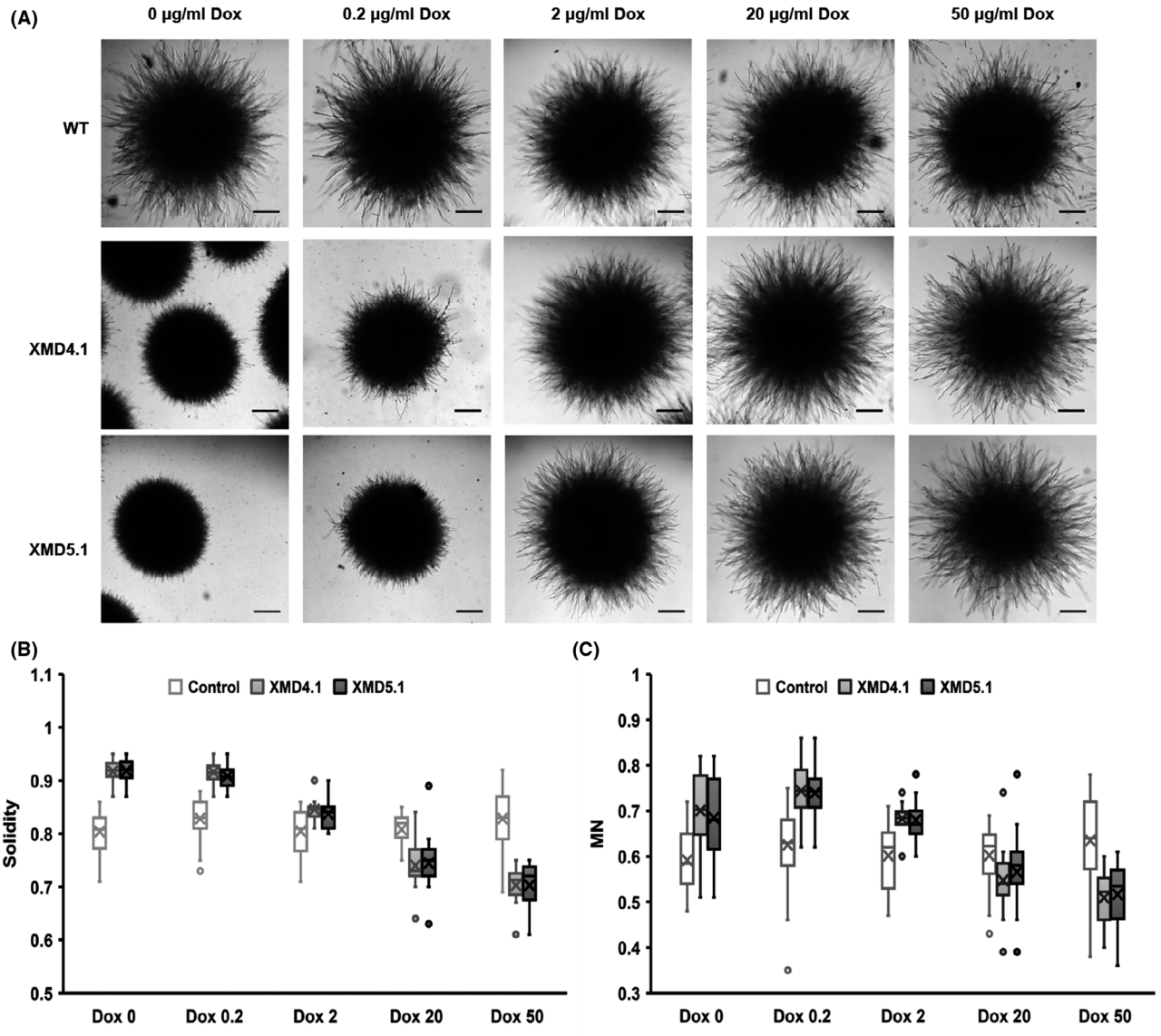

Fig. 2. Pellet morphological characteristics of *pkaC* conditional expression mutants. Representative images (A), the quantitative parameters solidity (B) and morphology number MN (C) of pellet morphology under submerged culture conditions. 1×10^5 spores ml^{-1} were inoculated in 20 ml citrate fermentation media supplemented with various concentrations of Dox and were incubated at 34°C in the dark for 24 h. Representative images are shown for technically triplicated experiments. Scale bar depicts 200 μm. WT, wild-type strain; XMD3.5, the *pkaC* disrupted mutant as positive control; XMD4.1 and XMD5.1, the *pkaC* conditional expression mutants.

against the citric acid titre (R^2 = 0.85, Fig. 3C) and normalized citric acid titre (R^2 = 0.85, Fig. 3D) respectively. Also, a very good correlation is obtained between the MN of all test cultivations and the citric acid production titre (R^2 = 0.81, Fig. 3E) and normalized citric acid titre (R^2 = 0.79, Fig. 3F) respectively. These data suggest that smaller pellet solidity and MN are important for high acid production and that this can be adjusted via *pkaC* expression in *A. niger*.

With regards to intracellular metabolite profile changes under different expression level of *pkaC*, metabolomics analyses of the progenitor control strain without Dox and *pkaC* conditional expression mutant XMD5.1 with various Dox concentrations were analysed by our established LC-MS/MS pipeline (Zheng *et al.*, 2019a). In detail, four samples were taken at the end of citric acid fermentation in shake flasks: progenitor control without Dox (II, *pkaC* normal expression), XMD5.1 without Dox (I, *pkaC* null expression), under 20 μg ml^{-1} Dox (III, *pkaC* overexpression) and under 50 μg ml^{-1} Dox (IV, *pkaC* hyperexpression) (Fig. 4). Nearly 100 intracellular metabolites were identified based on LC-MS/MS, including sugars, phosphorylated compounds, amino acids, organic acids and cofactors. To investigate the effects of *pkaC* expression,

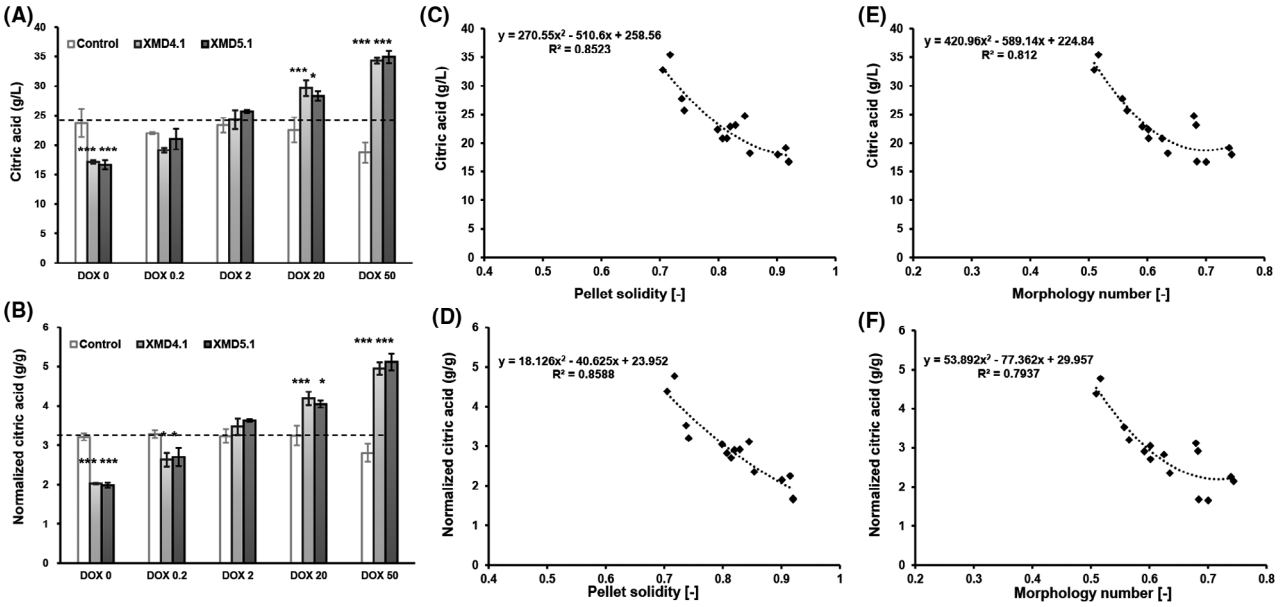

Fig. 3. Citric acid production and correlation to fungal morphology of *pkaC* conditional expression mutants in citric acid flask-shaking fermentation. Citric acid titre (A) and normalized citric acid titre against dry weight (B) of D353, XMD 4.1 and XMD5.1 cultivation under various concentrations of Dox. 1×10^5 spores ml^{-1} were inoculated in 20 ml citrate fermentation (CitFM) media supplemented with various concentrations of Dox and incubated at 34°C in the dark for 96 h. The extracellular acids were determined by the method of HPLC. Pairwise Student's *t*-tests were conducted between conditional expression mutant relative to the progenitor control at respective Dox concentrations. *P*-values are indicated as (< 0.05, *; < 0.01, **; < 0.001, ***). Citric acid titre (C) and normalized citric acid titre against dry weight (D) of all conducted cultivations under various concentrations of Dox are plotted over corresponding pellet solidity. Citric acid titre (E) and normalized citric acid titre against dry weight (F) of all conducted cultivations under various concentrations of Dox are plotted over corresponding MN. Each diamond represents a single cultivation for citric acid fermentation in shake flask.

relative levels of 30 metabolites involved in the central metabolism pathways were analysed in detail (Fig. 4). G6P and FBP significantly decreased when *pkaC* was overexpressed above physiological conditions, whereas glycerate 1,3-biphosphate and D-glycerate 3-phosphate/D-glycerate 2-phosphate significantly increased (Fig. 4). Glucose, ribulose 5-phosphate/ribose 5-phosphate and glycerine 3-phosphate/D-glyceraldehyde was only increased in the wild-type control. The important precursors of citric acid synthesis, pyruvate, acetyl-CoA and oxaloacetate showed no significant changes under different *pkaC* expression levels. For TCA cycle intermediates, except citric acid and malic acid, most intracellular intermediates level significantly decreased, especially for succinic acid and fumaric acid, when *pkaC* was overexpressed with 20 or 50 μg ml^{-1} Dox (Fig. 4). The intracellular citric acid gradually increased with the increase of the *pkaC* expression, which was consistent with the change of the extracellular citric acid. However, intracellular malic acid only slightly increased with 50 μg ml^{-1} Dox supplemented (Fig. 4). As to the amino acids, the intracellular levels of several detected amino acids decreased, such as lysine, threonine, histone and proline under the condition of high concentration of Dox, whereas glutamate and glutamine increased up to 30%, which suggested that the PkaC expression might also influence the amino acid metabolism, but the molecular basis of this change needs to be dissected in future. As for nucleotides and cofactors, both ATP and NADH significantly reduced upon *pkaC* overexpression. Taken together, the results confirm that the *pkaC* expression significantly affected the intracellular metabolite profile of *A. niger*, contributing to the intracellular citric acid accumulation resulting from the elevated *pkaC* expression.

Transcriptional coexpression analysis of pkaC *conditional expression mutants during citric acid production generates gene modules enriched with organic acid and morphology associated genes*

To unveil the transcriptional basis of *pkaC* hyperproductivity and pellet macromorphological changes, we generated a coexpression network from conditional expression mutant XMD5.1 in submerged citric acid fermentation with either 0, 0.2, 2, 20 or 50 μg ml^{-1} Dox (Table S5). After removing genes with low expression, a total of 9, 568 genes were used for network construction. The list of these genes and their log-transformed expression matrix is given in Table S6. WGCNA enables the identification of functional modules which are associated with sample traits (*e.g.* citric acid titres or pellet

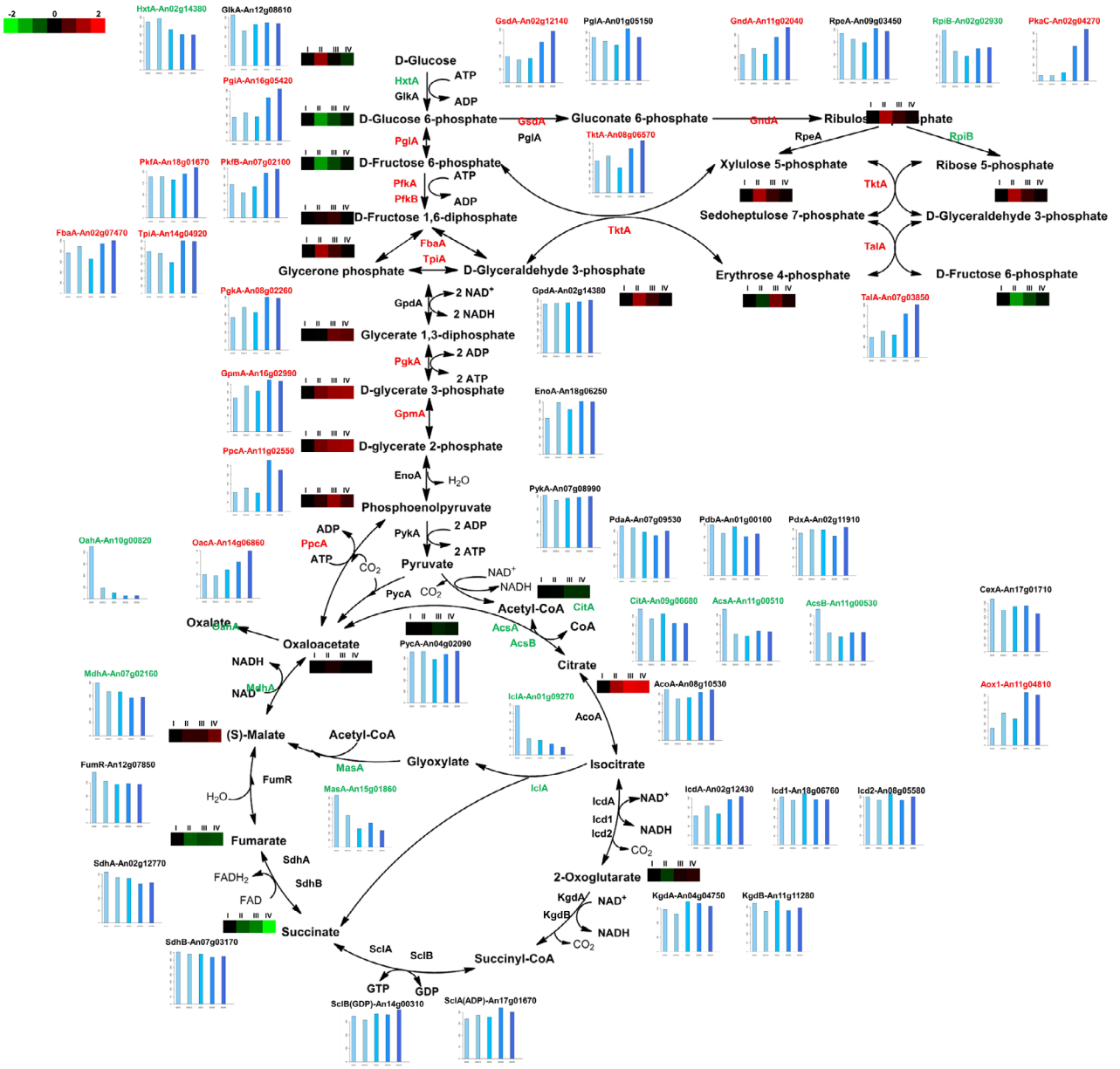

Fig. 4. Gene expression profiling of the enzymes and intracellular metabolite profiling of intermediates involved in central metabolic pathway in *pkaC* conditional expression mutants. Four samples of intracellular metabolite profiling were taken and analysed: progenitor control D353 (II), XMD5.1 without Dox (I), under 20 μg ml^{-1} Dox (III) and under 50 μg ml^{-1} Dox (IV). The peak intensity of each metabolite was first normalized against the total peak intensity within a sample. The relative level of each metabolite in a sample was calculated by dividing its normalized peak intensity by that of XMD5.1 without Dox (I). All metabolites' intensities were determined by triplicate technical measurements. The green blocks represented the intracellular level of this metabolite under different conditions which was lower than the ones without the addition of Dox. The gene expression level of each gene was calculated as Reads Per Kilobase Million (RPKM). The genes labelled in green were down-regulated the addition of Dox, while the genes labelled in red had a similar gene expression pattern to the *pkaC* gene. The genes labelled in black showed no significant change.

macromorphology). Additionally, WGCNA enables the delineation of so-called hub genes (highly connected genes) in the trait-related modules, thus identifying putative key or regulatory genes which are embedded in respective modules. The coexpression network generated via WGCNA in this study identified 33 coexpression modules of various size based on a dissimilarity measure (1-TOM) (Fig. 5 and Table S7). The 3348 genes in the turquoise module displayed a gradual increase in expression with the addition of Dox based on their eigengene profile, and, additionally, showed a high positive correlation with citric acid production with the

correlation coefficiency of 0.89 (*P*-value: 6E−04), and a negative correlation with pellet solidity (−0.97, *P*-value: 5E−06) and MN (0.98, *P*-value: 3E−07) (Fig. 5). The second key module was identified from this analysis (the blue module), which contained 1004 genes and was negatively correlated with acid production with the correlation coefficiency of −0.97 (*P*-value: 2E−06), yet positively correlated with pellet solidity (0.90, *P*-value: 4E−04) and MN (0.77, *P*-value: 9E−03) (Fig. 5). We therefore hypothesized that genes within the turquoise and blue modules, respectively, underpin the changes in citric acid titres and pellet surface structure observed following titration of *pkaC* expression.

Turquoise and blue modules were therefore further interrogated using GO and KOG enrichment analysis (Table S8). Consistent with the role of genes within the turquoise module as being involved in organic acid synthesis, GO analysis revealed primary metabolism, organic acid metabolic processes, and carboxylic acid processes were highly enriched, among others (FDR $P < 0.001$). Notably, this included the genes encoding citric acid synthase *citA* (An09g06680) and two isocitrate dehydrogenases (*icdA*, An02g12430 and An08g05580). Moreover, this module was enriched with genes associated with the mitochondria ($P = 0.001$), further supporting the role of this module in organic acid synthesis.

The hypothesis that genes within the blue module impact pellet surface structure was also supported by GO analysis, which revealed enrichment of genes associated with the cell periphery (FDR $P = 0.003$) and anchored components of the plasma membrane (FDR $P = 0.01$). This includes genes encoding putative chitin synthases (*chsB* (An09g04010), *chsD* (An09g02290), *chsL* (An02g02340), *chsM* (An02g02360)), beta glucanases (An01g04560 and An11g01540), 1,3-beta-glucanosyltransferase *gelF* (An16g06120), glycosylphosphatidylinositol (GPI)-anchored cell wall mannoprotein

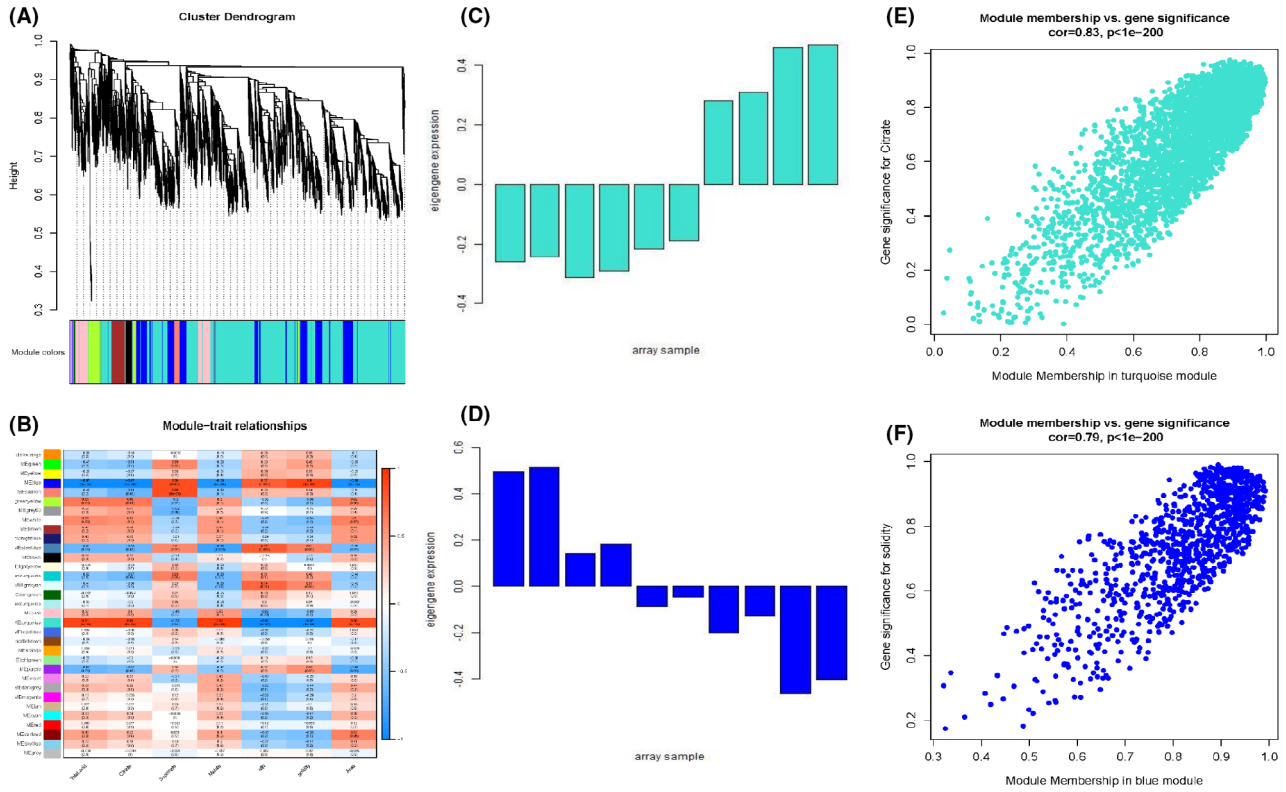

Fig. 5. Weighted gene coexpression network analysis (WGCNA) analysis of pkaC conditional expression mutant with different concentration of Dox.

A. Gene hierarchical clustering dendrogram based on a dissimilarity measure (1-TOM), which showed 38 coexpression modules with different colours identified by WGCNA. Each branch in the tree represents an individual gene. The height (*y*-axis) indicates the coexpression distance and the *x*-axis corresponds to genes.

B. Module–trait relationships. ME means the module eigengene. Each row corresponds to a module. Each column corresponds to different traits involved in citric acid production and morphology. The colour of each cell at the row-column intersection indicates the correlation coefficient between the module and the traits. A high degree of correlation coefficiency is indicated by dark red or dark blue. The scale on the right represents the correlation range from positive (red, 1) to negative (blue, −1). The gene expression patterns in MEturquoise (C) and MEblue modules (D).

cwpA (An14g02100), other GPI-anchored proteins (e.g. glucanosyltransferase *chrC* (An07g01160)) and various cell wall growth/integrity regulators, notably the Rho GTPase *rhoC* (An14g05530) and heterotrimeric G-protein alpha-subunit *fadA* (An08g06130). It is therefore reasonable to speculate that differential expression of these genes in the *pkaC* mutant impact cell wall synthesis or integrity, thus causing changes to hyphal growth at the surface of the pellet. Taken together, these data support the hypothesis that elevated expression of genes within turquoise module facilitate the elevated titres of citric acid production following *pkaC* expression. Additionally, we hypothesize that blue module reveals a shortlist of high-priority targets for rational morphological engineering in *A. niger* to achieve elevated citric acid titres.

In silico *identification of hub genes from two key coexpression modules*

To identify hub genes involved in citric acid production and pellet morphology, genes in the turquoise and blue modules were further examined to assess their topological behaviour in terms of module membership (MM) and gene significance (GS) of citric acid production, pellet solidity and MN value (Fig. 5 and Fig. S4). A total number of 1016 and 387 hub genes were identified in turquoise and blue modules respectively (Table S9). These identified hub genes were also analysed for GO biological processes and KOG enrichment. The hub genes were enriched in cell signalling, transcription and biological processes. KOG pathway enrichment analysis revealed that genes in this module were enriched in carbohydrate transport and metabolism (*P*-value: 4.51E−05, FDR: 0.032) (Table S10).

To further identify the key regulators involved in cell signalling and transcription regulation, the expression pattern and biological function of hub genes were investigated in details, in combination of protein–protein interaction network analysis. As shown in Tables S11 and 12, 40 and 9 key regulators were identified in the turquoise and blue module respectively. Among them, 21 hub genes were found in the protein–protein interaction network, wherein 18 regulators showed direct interaction with PkaC, such as three components in cAMP-PKA signalling pathway and two components in the HOG-MAPK signalling pathway. Moreover, the expression level of the genes involved in signalling pathway and hub regulators was showed in Fig. S5. The components in cAMP-PKA signalling pathway, including *fadA* (An08g06130), *pkaR* (An16g03740), *flbA* (An02g03160), *rgsA* (An18g06110), showed the comparable expression patterns with the increasing *pkaC* expression (Fig. S5). Moreover, two key components in the high-osmolarity glycerol response mitogen-activated protein kinase (HOG-MAPK) signalling pathway, *hogA* (An08g05850) and *mpkC* (An18g05270), also displayed the coexpression pattern with *pkaC* (Fig. S5).

Consistent with the hypothesis that the turquoise module drives citric acid synthesis, the hub genes were enriched in the carbohydrate transport and metabolism (Table S10). In order to elucidate the profile changes under different expression level of *pkaC*, the expression level of the genes involved in central metabolism was analysed in detail (Fig. 4). Along with the increase of *pkaC* expression, except hexokinase gene *hxkA* (An02g14380) and ribose 5-phosphate isomerase gene *rpiB*, the expressions of most of the genes in the glycolysis and pentose phosphate pathway were up-regulated, especially the two genes using glucose 6-phosphate (the intersection of the glucose metabolism) as substrate, glucose 6-phosphate isomerase gene *pgiA* (An16g05420) and glucose 6-phosphate dehydrogenase gene *gsdA* (An02g12140). The 6-phosphofructo-1-kinase gene *pfkA* (An18g01670) catalysed the rate-limiting step of glycolysis which was up-regulated when *pkaC* was overexpressed with 20 and 50 μg ml− Dox. Meanwhile, the 6-phosphofructo-2-kinase gene *pfkB*, which converts D-fructose 6-phosphate into D-fructose 2, 6-bisphosphate (the allosteric activator of *pkfA*), was also significantly up-regulated. Pyruvate kinase gene *pkiA* (An07g08990) and pyruvate carboxylase *pycA* (An04g02090) have no significant change, but the phosphoenolpyruvate carboxykinase gene *ppcA* (An11g02550) was dramatically up-regulated. As to the citric acid precursor oxaloacetate, the oxaloacetate transporter gene *oacA* (An14g06860) was significantly up-regulated, while the gene encoding cytoplasmic oxaloacetate acetyl-hydrolase *oahA* (An10g00820), which catalysed oxaloacetate into oxalic acid, was significantly down-regulated. Genes involved in TCA cycle have no significant changes, except the *citA* gene (An09g6680) and the *mdhA* gene (An07g02160) with slight downregulation with the increase gene expression of *pkaC*. The citric acid exporter *cexA* gene (An17g01710) showed the similar expression pattern, while the alternative oxidase Aox1 (An11g04810) displayed opposite trend. Besides, the two genes involved in glyoxylate bypass, iso-citrate lyase *iclA* (An01g09270) and malate synthase *masA* (An15g01860), were also significantly down-regulated. Moreover, cytoplasmic ATP citrate lyase genes, *aclA* (An11g00510) and *aclB* (An11g00530), were down-regulated once the *pkaC* gene was expressed. These results demonstrated that *pkaC* played a vital role in the regulation of central metabolism.

Finally, consistent with the role of the cell wall in controlling pellet surface structure, hub genes in the blue module contained several genes encoding chitin

syntheses involved in cell wall biosynthesis. The genes encoding *chsB* (An09g04010), *chsD* (An09g02290), *chsL* (An02g02340), *chsM* (An02g02360) were significantly down-regulated in the addition of Dox (Fig. S6). We consider hub genes to be high-priority candidates for morphological engineering in *A. niger* and other fungi.

Discussion

Filamentous fungi are widely exploited as cell factories in the production of organic acids, proteins and enzymes (Meyer, 2008; Lubertozzi and Keasling, 2009; Meyer *et al.*, 2011b). It is clear that pellet morphology in submerged fermentation dramatically impacts the production capability in industrial bioprocesses (Krull *et al.*, 2013; Cairns *et al.*, 2019c; Chen *et al.*, 2019). Given that cell signalling cascades play an essential role in filamentous growth and are generally conserved, studies of their respective components will provide potential targets for morphology engineering among many industrially utilized fungi (Cairns *et al.*, 2019c). The protein kinase A (PKA)/-cyclic adenosine monophosphate (cAMP) is a signalling cascade of fundamental importance to the filamentous lifestyle, which regulates both vegetative growth and carbon sensing (Bencina *et al.*, 1997; Saudohar *et al.*, 2002). As an important component of cAMP signalling pathway, the *pkaC* gene was first studied in *A. niger* by Bencina *et al.*, who performed *pkaC* overexpression studies (Bencina *et al.*, 1997). Interestingly, these authors found that the phenotypes of compact colony morphology and defective sporulation varied among different transformants, which we presume is due to the random integration of the *pkaC* gene cassette. Since this initial study, no research to date has comprehensively determined the role of *pkaC* for submerged growth and organic acid productivity.

In this study, we demonstrate that *pkaC* disruption results multiple defects in growth at hyphal, colony and submerged pellet level. We also found that the *pkaC* disruption affected polarity establishment and resulted in increased hyphal branch frequency in *A. niger* (Fig. 1), which might be the causatively linked to more compact pellets with the less emanated hypha surrounding the pellets (Fig. 2). Encouragingly, modifications to pellet growth parameters following artificial *pkaC* expression were reproducible within cultures and did not result in an increase in culture heterogeneity, an observation we have found following modified expression of other morphology associated genes in *A. niger*. These data indicate that pellet morphology of *A. niger* can be rationally and robustly modulated by controlling *pkaC* expression levels.

From an applied perspective, both intracellular and secreted citric acid titres increased following *pkaC* overexpression, identifying this as a promising target to maximize efficiency during industrial fermentation. A growing body of work has determined the qualitative correlation between morphology and production in submerged fermentation, for instance, macromorphology and fumarate production (Zhou *et al.*, 2011), gluconic acid production (Lu *et al.*, 2015), itaconate production (Kuenz *et al.*, 2012) and malic acid production (Chen *et al.*, 2019). Data from this study suggest that modifications to pellet morphology at the surface are crucial for increased extracellular titres of citric acid. The pellet surface can be modulated by titrated expression of *pkaC*, with solidity in this study ranging from 0.9 to 0.7, with good correlation to citric acid production increasing up to 1.87-fold. It is possible that the more extensive growth of hypha at the periphery may result in a looser outer pellet layer, thus enable better mass transfer of oxygen, nutrients and secreted products, a hypothesis consistent with nutrient diffusion being recently confirmed as a crucial limitation for productivity and growth in *A. niger* and other fungi. Thus, we identify *pkaC* as a crucial hub regulator that links cell morphology control and citric acid production.

To unveil the *pkaC* regulation network involved in the morphology and citric acid production, the trait-correlated coexpression network was analysed by approach of WGCNA on the expression profiles of *pkaC* titratable expression mutants. WGCNA represents a recently developed approach that enables network construction from smaller number of transcriptional datasets, and, additionally, the quantitative correlation of gene expression modules with phenotypes of interest. Among the identified 33 modules, two modules displayed the highest correlations with the citric acid production and pellet morphology (Fig. 5) which enable identification of various other putative hub regulators which are priority targets for further strain engineering studies given their modulated expression in optimized pellet and productive growth (Tables S11 and S12, Fig. S5). These hub regulators and the *pkaC* regulation network were constructed as depicted in Fig. 6 and Fig. S6, which includes other signalling components (e.g. *fadA*, *pkaR*, *flbA* and *rgsA*). Interestingly, two key components in the HOG-MAPK signalling pathway, *hogA* and *mpkC,* also displayed the coexpression pattern with *pkaC* (Fig. S5), confirming this pathway is also a priority target for strain engineering in *A. niger*. It is also interesting that several components of the cell wall integrity signalling pathways, such as *wscA* and *rhoA*, showed a similar trend with the expression pattern of several chitin synthases (Figs S5 and S6), but an opposite trend to *pkaC* gene expression. As shown in Fig. 6, these data are consistent with PKA/cAMP signalling pathway that played a hub regulatory role in hyphal development, cell wall synthesis and pellet

morphology by cross-talk with the HOG-MAPK pathway (Gutin *et al.*, 2015; de Assis *et al.*, 2018; Urita *et al.*, 2021) and CWI pathway (Donlin *et al.*, 2014; García *et al.*, 2017) in other fungi.

From a metabolic perspective, this study demonstrated that *pkaC* overexpression increased both extracellular and intracellular citric acid. As shown in Fig. 4, most of the genes involved in glycolysis were up-regulated following *pkaC* overexpression. Kuang *et al* also reported that Msn2/4 regulated the expression of glycolytic enzymes in yeast (Kuang *et al.*, 2017). An orthologous transcription factor (An07g05960) of Msn2p was identified as the hub regulator by coexpression analysis, which may make the bridge between *pkaC* and glycolysis regulation (Fig. 6 and Fig. S5). Moreover, we observed that *pkaC* could also enhance the import of citric acid precursor oxaloacetate into mitochondria by upregulation of oxaloacetate transporter *oacA* and improved the oxaloacetate supplement by downregulation of cytoplasmic oxaloacetate acetyl-hydrolase *oahA* and glyoxylate bypass. Although the citrate synthase *citA* and citrate exporter *cexA* (Steiger *et al.*, 2019) showed slight decreased expression when *pkaC* was overexpression, the alternative oxidase Aox1 was significantly up-regulated (Fig. 4). It indicated that *pkaC* may not involve in the direct regulation of citric acid synthesis and transport. To sum up, the results suggest that *pkaC* plays a key role in the regulation of glycolysis, the oxaloacetate supplement and alternative electron transport chain, resulting in the accumulation of extracellular citric acid.

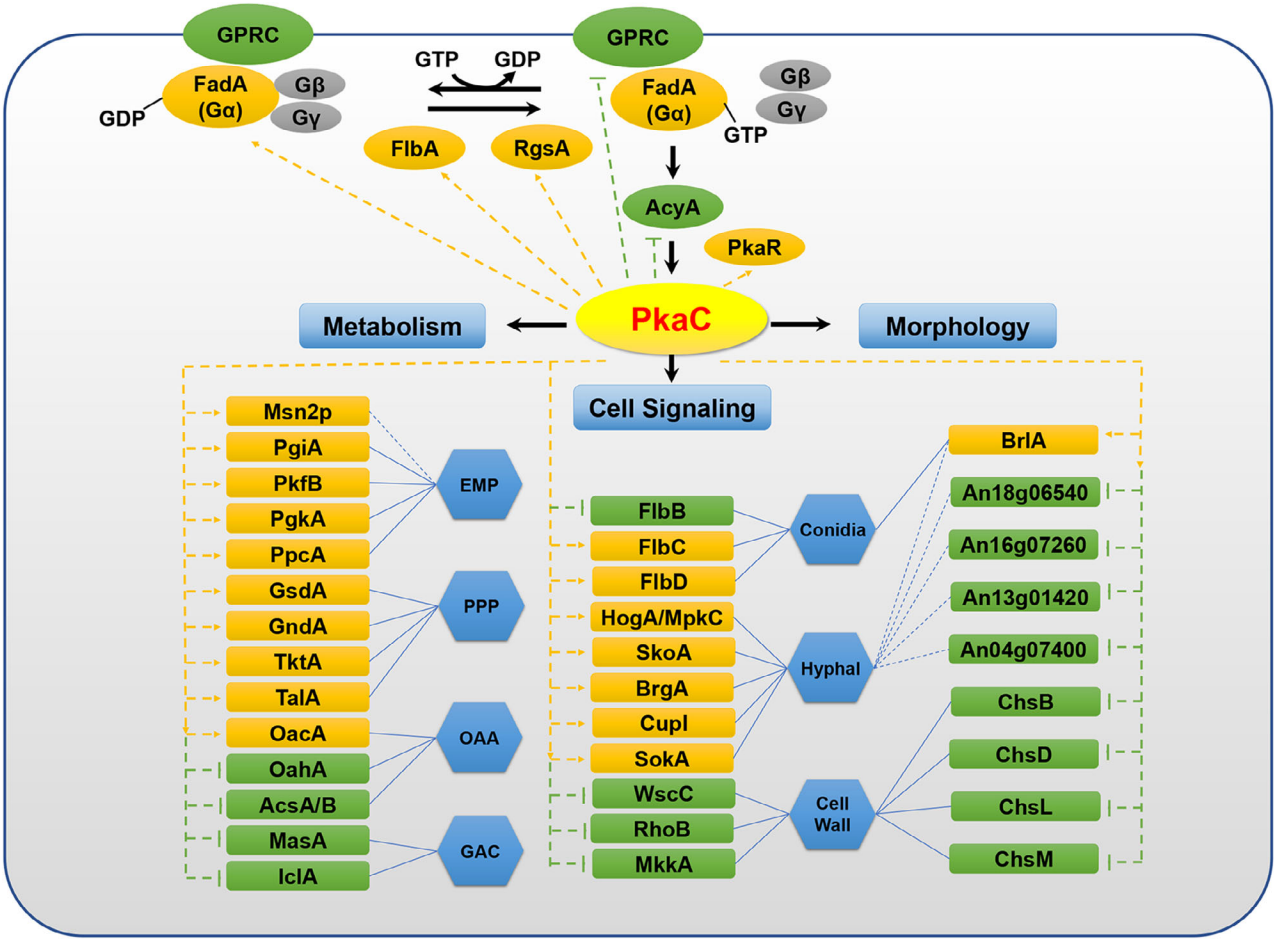

Fig. 6. Predicted regulation network of *pkaC* based on the coexpression analysis. It demonstrated that the protein kinase PkaC could be the hub regulator involved in cell signalling, cell metabolism and morphology (blue boxes). The genes labelled in green boxes were down-regulated with opposite gene expression pattern of *pkaC*, while the genes labelled in yellow boxes were up-regulated by *pkaC*. The components in cAMP-PKA signalling pathway were shown in green circles (down-regulated), yellow circles (up-regulated) and grey circles (not-regulated). EMP, Embden–Meyerhof–Parnas pathway; GAC, glyoxylic acid cycle; OAA, oxaloacetic acid transport and metabolism; PPP, pentose phosphate pathway.

Conclusion

This study demonstrates that PkaC is a promising target to elevate citric acid fermentation titres using *A. niger*. Data presented in this study demonstrate *pkaC* overexpression increases glycolytic flux, while concomitantly modifying hyphal growth at the pellet surface which may improve nutrient transfer. WGCNA analysis generates several coexpression modules which were enriched with high-priority hub genes for future strain engineering projects. Future studies of fungal cell signalling pathways including cAMP/PKA signalling will likely provide fundamental insights into complex metabolic and morphological regulatory mechanisms and will disclose more potential targets for engineering the next generations of highly efficient fungal cell factories.

Experimental procedures

Strains and culture conditions

The *A. niger* strains used in this study are listed in Table S1. *Escherichia coli* DH5α (Transgene, Beijing, China) was used for plasmid construction and cultured at 37°C in Luria–Bertani broth containing ampicillin (100 μg ml^{-1}). The citric acid producing strains *A. niger* D353 was purchased from Shanghai Industrial Microbiology Institute Tech. Co. (Shanghai, China), with the collection number M203. *A. niger* strains were cultivated on defined minimal medium (MM) as reported previously (Carvalho *et al.*, 2010), or on complete medium (CM) consisting of MM supplemented with 0.5% yeast extract and 0.1% casamino acids. 1.5% agar was supplemented for plates. When necessary, 150 μg ml^{-1} of hygromycin was added for the *hph* selection marker.

Plasmid and strain construction

All protospacers, primers and plasmids used in this study are listed in Tables S2–S4 respectively. To construct the sgRNA targeting different genes, protospacers were first predicted sgRNA by the sgRNAcas9 software (Xie *et al.*, 2014) and designed with minimal off-target possibility (Table S2). The targeting sgRNA constructs were built by digestion of sgRNA expression plasmids psgRNA6.0 (Zheng *et al.*, 2019b) with *Bbs*I, and ligation with synthetic double-stranded oligonucleotides of the desired sequences (Zheng *et al.*, 2019b). The donor DNAs with microhomology (40-bp) flanks were generated as previously described (Zheng *et al.*, 2019b). The linear donor DNA MHi-pkaC3-hph and MHr-pkaC1/2-hyh:Tet-on/ MHi-pkaC2-hph:Tet-on were amplified with pSilent-1(Nakayashiki *et al.*, 2005) and pTC1.13 as template with corresponding primers respectively. The standard protocol of *A. niger* genome editing using the CRISPR/Cas9 system-based 5S rRNA was performed as previously described (Zheng *et al.*, 2019b). For *pkaC* gene insertion, 2 μg sgRNA-pkaC3 constructs, 2 μg donor DNA constructs MHi-pkaC3-Hph and pCas9-hph (Zhang *et al.*, 2020) into the protoplasts of *A. niger* D353. To construct the *pkaC* inducible expressed mutants, two genome editing strategies were carried out: (1) replace the native promoter P*pkaC* with Tet-on system by induced two-DBSs flanking the P*pkaC*; (2) insert the Tet-on system in the upstream of the *pkaC* coding sequences. After twice subculture and purification, genomic DNA of random selected transformants was extracted and verified via diagnostic PCR and sequencing analysis with the corresponding primers (Table S4).

Phenotypic screening on solid medium

Phenotypic detection was carried out as described previously (Cairns *et al.*, 2019b). Briefly, *A. niger* conidia were harvested from 5-day cultivated CM agar plates. For *pkaC* conditional expression mutants, 20 μg ml^{-1} Dox was supplemented in CM agar plates with hygromycin. Spores were harvested in0.9% NaCl solution and filtered through Miracloth. Spores of *A. niger* isolates were spotted with 2 μl volumes at concentration of 1×10^3 and 1×10^4 spores ml^{-1} on CM and MM agar plates with 0, 2 and 20 μg ml^{-1} Dox, which were incubated for 3 days at 30°C. For phenotypic screens under high osmotic stress, MM plates were supplemented with 1 M sorbitol. All experiments were conducted in technical triplicate.

Morphological characteristics via scanning electron microscopy (SEM)

Morphological characteristics of conidiophores and conidia were performed using a scanning electron microscope (Hitachi SU8010, Japan). Conidiophores were cultured for 3 days at 30°C on CM plates with 0, 2 and 20 μg ml^{-1} Dox, while the conidia were cultured for 5 days with the same condition. The samples were directly taken and put on the adhesive tape, and then coated with gold and observed by SEM.

Quantitative assessment of mycelial pellet morphology

The mycelial pellet morphology was quantitatively observed as described previously (Cairns *et al.*, 2019b) with minor modification. Briefly, the mycelial pellets of citric acid fermentation were observed using Zeiss Axioscope 5 microscope. To keep the mycelial pellet state, cultures were put on the glass slide without cover glass. For each sample, six images were captured from randomly selected. Mycelial pellet morphologies were quantified in ImageJ/Fiji using the morphology of dispersed

and pelleted growth (MPD) plugin (Cairns *et al*., 2019b). For each mycelial pellet, the following parameters were calculated: area (μm^2), Feret's diameter (maximum diameter of each structure, μm), aspect ratio (maximum diameter/minimum diameter) and solidity. Morphology numbers (MNs) were also calculated as described (Wucherpfennig *et al*., 2011; Cairns *et al*., 2019b).

Citric acid fermentation and metabolite detection

Citrate fermentation was carried out using the liquefied corn media (Zheng *et al*., 2019a). The final concentration of 1×10^5 spores ml^{-1} was inoculated in 20 ml liquefied corn media with 0, 0.2, 2, 20 and 50 $\mu g\ ml^{-1}$ Dox in 100 ml shake flasks, which were cultivated at 34°C and 220 rpm for 96 h. The weight of the shake flasks was measured before and after the citric acid fermentation to eliminate measurement errors caused by evaporation. Extracellular organic acids were detected by Prominence UFLC equipped with a UV detector (Shimadzu, Kyoto, Japan) and a Bio-Rad Aminex HPX-87H column (300 × 7.8 mm) according to the procedure described previously (Zhang *et al*., 2020). A minimum of three shake flask cultures were analysed for each strain and Dox concentration. The samples for intracellular metabolite profiling were prepared and detected by the LC-MS/MS platform containing ultra-performance liquid chromatography (UPLC) 30A (Shimadzu, Kyoto, Japan) and TripleTOF™ 6600 mass spectrometer (Applied Biosystems Sciex, USA), according to the standardized and improved LC-MS/MS metabolomics methodology (Zheng *et al*., 2019a).

RNA sequencing and transcriptomics analysis

The mycelial pellet samples were collected by rapid vacuum filtration after cultivating for 48 h at 34°C in 20 ml liquefied corn media with 0, 0.2, 2, 20 or 50 $\mu g\ ml^{-1}$ Dox with the final concentration of 1×10^5 spores ml^{-1}. After collection, the samples were washed with 100 ml cold sterilized water and then immediately placed into liquid nitrogen and stored at −80°C. Total RNAs were extracted using RNAprep pure Plant Kit (DP432, Tiangen, Beijing, China) according to the manufacturer's instruction. RNA concentration and purity were measured using NanoDrop 2000 (Thermo Fisher Scientific, Wilmington, Germany). RNA integrity was assessed using the RNA Nano 6000 Assay Kit of the Agilent Bioanalyser 2100 system (Agilent Technologies, CA, USA). Sequencing libraries were constructed using NEBNext UltraTM RNA Library Prep Kit for Illumina (NEB, USA), the library preparations were sequenced on an Illumina platform, and paired-end reads were generated at Beijing Biomarker Technology (Beijing, China). A total of 503 545 786 clean reads related to 10 cDNA libraries (each condition measured in duplicate) were obtained for assembly and further analysis after filtering and trimming the raw data (Table S5). Average clean reads of 52.22, 50.02, 51.43, 50.14 and 47.96 million were generated from the samples under the concentration of 0, 0.2, 2, 20 and 50 $\mu g\ ml^{-1}$ Dox. The percentage of bases with Phred scores at the Q30 level (an error probability of 1‰) ranged from 93.75% to 94.20%, and the GC content was 54.16%. Among all the samples, 93.51–94.47% of the clean reads were mapped to the reference genome, in which 92.87–93.87% of clean reads were uniquely mapped (Table S5). Clean reads were obtained by removing reads containing adapter, reads containing ploy-N and low-quality reads from the raw reads. These clean reads were then mapped to the reference genome sequence of the progenitor strain which was annotated according to the reference genome of *A. niger* CBS 513.88 (Accession: PRJNA19263). These data have been provided in the supplementary materials.

Weighted gene coexpression network analysis (WGCNA) was performed using the R package (version 1.69, https://horvath.genetics.ucla.edu/html/CoexpressionNetwork/Rpackages/WGCNA/) with these transcriptomic data shown in Table S6 (Langfelder and Horvath, 2008). First, the reliability of samples and genes for WGCNA analysis was inspected to exclude the genes with zero variance. To construct the scale-free network, an appropriate soft thresholding power β was calculated by plotting the R^2 (scale-free topology fitting index) against soft thresholds. At $\beta = 9$, network created by WGNCA showed > 90% scale-free topology. Then, the coexpression modules were constructed using automatic module detection function blockwise with default settings except the soft thresholding power was 9, the min module size was 30, and the merge cut height was 0.25. Finally, the modules were then associated with the phenotypic parameters of citric acid fermentation and pellet morphology to obtain important modules related to the citric acid production and morphological regulation of *A. niger*. Generally, the hub genes with the highest degree of connectivity in the module was considered as the key genes that play an important role in the given phenotype. The screening criteria for hub genes in the interesting modules were identified as the value of module membership (MM > 0.8) and the absolute value of gene significance (|GS| > 0.2) in interesting traits.

Gene ontology (GO) enrichment analysis of the genes in the modules and the hub genes was then performed to obtain significant GO terms. Fisher's exact test, which is based on the hypergeometric distribution, was used to calculate the p-value, and GO terms with a corrected p-value less than 0.05 were considered to be significantly enriched. Where indicated, GO enrichment analysis of

biological process or cellular components was performed using FungiDB, with false discovery corrected *p*-values computed using the Benjamini method (Stajich *et al.*, 2012). The protein–protein interaction (PPI) network of the hub genes was constructed by using the Search Tool for the Retrieval of Interacting Genes (STRING) database (http://string-db.org/) (von Mering *et al.*, 2003), with the interaction score of medium confidence > 0.4, which was deemed to be statistically significant. CYTOSCAPE (version 3.7.0) (Shannon *et al.*, 2003) was used to visualize the network.

Acknowledgments

This study was supported by the National Key R&D Programme of China (2018YFA0900500), National Natural Sciences Foundation of China (31961133021 and 32070082), Tianjin Synthetic Biotechnology Innovation Capacity Improvement Project (TSBICIP-PTJS-003), Deutsche Forschungs gemeinschaft (DFG) for the financial support for this work grant ME 2041/13-1.

Author contributions

X.Z., P.Z. and J.S. conceived the study. X.Z., X.N. and L.Z. performed the experiments. H.Z took part in the SEM analysis. X.Z. and T.C. drafted and revised the manuscript. P.Z., J.S. and V.M. revised the manuscript. All authors approved the manuscript.

Conflicts of interest

The authors declare no conflict of interest.

References

de Assis, L.J., Manfiolli, A., Mattos, E., Fabri, J., Malavazi, I., Jacobsen, I.D., *et al.* (2018) Protein Kinase A and high-osmolarity glycerol response pathways cooperatively control cell wall carbohydrate mobilization in *Aspergillus fumigatus*. *mBio* **9:** e01952–18.

de Assis, L.J., Ries, L.N., Savoldi, M., Dos Reis, T.F., Brown, N.A., and Goldman, G.H. (2015) *Aspergillus nidulans* protein kinase A plays an important role in cellulase production. *Biotechnol Biofuels* **8:** 213.

Bencina, M., Panneman, H., Ruijter, G.J., Legisa, M., and Visser, J. (1997) Characterization and overexpression of the *Aspergillus niger* gene encoding the cAMP-dependent protein kinase catalytic subunit. *Microbiology* **143(Pt** 4): 1211–1220.

Bizukojc, M., and Ledakowicz, S. (2009) Physiological, morphological and kinetic aspects of lovastatin biosynthesis by *Aspergillus terreus*. *Biotechnol J* **4:** 647–664.

Bizukojc, M., and Ledakowicz, S. (2010) The morphological and physiological evolution of *Aspergillus terreus* mycelium in the submerged culture and its relation to the formation of secondary metabolites. *World J Microb Biotechnol* **26:** 41–54.

Brown, N.A., Dos Reis, T.F., Ries, L.N., Caldana, C., Mah, J.H., Yu, J.H., *et al.* (2015) G-protein coupled receptor-mediated nutrient sensing and developmental control in *Aspergillus nidulans*. *Mol Microbiol* **98:** 420–439.

Cairns, T.C., Feurstein, C., Zheng, X., Zhang, L.H., Zheng, P., Sun, J., and Meyer, V. (2019a) Functional exploration of co-expression networks identifies a nexus for modulating protein and citric acid titres in *Aspergillus niger* submerged culture. *Fungal Biol Biotechnol* **6:** 18.

Cairns, T.C., Feurstein, C., Zheng, X., Zheng, P., Sun, J., and Meyer, V. (2019b) A quantitative image analysis pipeline for the characterization of filamentous fungal morphologies as a tool to uncover targets for morphology engineering: a case study using aplD in *Aspergillus niger*. *Biotechnol Biofuels* **12:** 149.

Cairns, T.C., Zheng, X., Zheng, P., Sun, J., and Meyer, V. (2019c) Moulding the mould: understanding and reprogramming filamentous fungal growth and morphogenesis for next generation cell factories. *Biotechnol Biofuel* **12:** 77.

Cairns, T.C., Nai, C., and Meyer, V. (2018) How a fungus shapes biotechnology: 100 years of *Aspergillus niger* research. *Fungal Biol Biotechnol* **5:** 13.

Carvalho, N.D., Arentshorst, M., Jin Kwon, M., Meyer, V., and Ram, A.F. (2010) Expanding the *ku70* toolbox for filamentous fungi: establishment of complementation vectors and recipient strains for advanced gene analyses. *Appl Microbiol Biotechnol* **87:** 1463–1473.

Casas Lopez, J.L., Sanchez Perez, J.A., Fernandez Sevilla, J.M., Rodriguez Porcel, E.M., and Chisti, Y. (2005) Pellet morphology, culture rheology and lovastatin production in cultures of *Aspergillus terreus*. *J Biotechnol* **116:** 61–77.

Chen, X., Zhou, J., Ding, Q., Luo, Q., and Liu, L. (2019) Morphology engineering of *Aspergillus oryzae* for l-malate production. *Biotechnol Bioeng* **116:** 2662–2673.

Choi, Y.H., Lee, N.Y., Kim, S.S., Park, H.S., and Shin, K.S. (2020) Comparative characterization of G protein α subunits in *Aspergillus fumigatus*. *Pathogens* **9:** 272.

Dai, Z., Mao, X., Magnuson, J.K., and Lasure, L.L. (2004) Identification of genes associated with morphology in *Aspergillus niger* by using suppression subtractive hybridization. *Appl Environ Microbiol* **70:** 2474–2485.

Dhillon, G.S., Brar, S.K., Verma, M., and Tyagi, R.D. (2011) Recent advances in citric acid bio-production and recovery. *Food Bioprocess Tech* **4:** 505–529.

Donlin, M.J., Upadhya, R., Gerik, K.J., Lam, W., VanArendonk, L.G., Specht, C.A., *et al.* (2014) Cross talk between the cell wall integrity and cyclic AMP/protein kinase A pathways in *Cryptococcus neoformans*. *MBio* **5:** e01573-14.

García, R., Bravo, E., Diez-Muñiz, S., Nombela, C., Rodríguez-Peña, J.M., and Arroyo, J. (2017) A novel connection between the Cell Wall Integrity and the PKA pathways regulates cell wall stress response in yeast. *Sci Rep* **7:** 5703.

Gomez, R., Schnabel, I., and Garrido, J. (1988) Pellet growth and citric acid yield of *Aspergillus niger* 110. *Enzyme Microbial Technol* **10:** 188–191.

Grosse, C., Heinekamp, T., Kniemeyer, O., Gehrke, A., and Brakhage, A.A. (2008) Protein kinase A regulates growth,

sporulation, and pigment formation in *Aspergillus fumigatus*. *Appl Environ Microbiol* **74:** 4923–4933.

Gutin, J., Sadeh, A., Rahat, A., Aharoni, A., and Friedman, N. (2015) Condition-specific genetic interaction maps reveal crosstalk between the cAMP/PKA and the HOG MAPK pathways in the activation of the general stress response. *Mol Syst Biol* **11:** 829.

Henzler, H.J. (2000) Particle stress in bioreactors. *Adv Biochem Eng Biotechnol* **67:** 35–82.

Karaffa, L., and Kubicek, C.P. (2003) *Aspergillus niger* citric acid accumulation: do we understand this well working black box? *Appl Microbiol Biotechnol* **61:** 189–196.

Krull, R., Wucherpfennig, T., Esfandabadi, M.E., Walisko, R., Melzer, G., Hempel, D.C., *et al*. (2013) Characterization and control of fungal morphology for improved production performance in biotechnology. *J Biotechnol* **163:** 112–123.

Kuang, Z., Pinglay, S., Ji, H.K., and Boeke, J.D. (2017) Msn2/4 regulate expression of glycolytic enzymes and control transition from quiescence to growth. *eLife* **6:** 29938.

Kuenz, A., Gallenmuller, Y., Willke, T., and Vorlop, K.D. (2012) Microbial production of itaconic acid: developing a stable platform for high product concentrations. *Appl Microbiol Biotechnol* **96:** 1209–1216.

Langfelder, P., and Horvath, S. (2008) WGCNA: an R package for weighted correlation network analysis. *BMC Bioinformatics* **9:** 559.

Legisa, M., and Mattey, M. (2007) Changes in primary metabolism leading to citric acid overflow in *Aspergillus niger*. *Biotech Lett* **29:** 181–190.

Liu, Y., Liao, W., and Chen, S.L. (2008) Study of pellet formation of filamentous fungi *Rhizopus oryzae* using a multiple logistic regression model. *Biotechnol Bioeng* **99:** 117–128.

Lu, F., Ping, K.K., Wen, L., Zhao, W., Wang, Z.J., Chu, J., and Zhuang, Y.P. (2015) Enhancing gluconic acid production by controlling the morphology of *Aspergillus niger* in submerged fermentation. *Process Biochem* **50:** 1342–1348.

Lubertozzi, D., and Keasling, J.D. (2009) Developing *Aspergillus* as a host for heterologous expression. *Biotechnol Adv* **27:** 53–75.

von Mering, C., Huynen, M., Jaeggi, D., Schmidt, S., Bork, P., and Snel, B. (2003) STRING: a database of predicted functional associations between proteins. *Nucleic Acids Res* **31:** 258–261.

Meyer, V. (2008) Genetic engineering of filamentous fungi-progress, obstacles and future trends. *Biotechnol Adv* **26:** 177–185.

Meyer, V., Cairns, T., Barthel, L., King, R., Kunz, P., Schmideder, S., *et al*. (2021) Understanding and controlling filamentous growth of fungal cell factories: novel tools and opportunities for targeted morphology engineering. *Fungal Biol Biotechnol* **8:** 8.

Meyer, V., Wanka, F., van Gent, J., Arentshorst, M., van den Hondel, C.A., and Ram, A.F. (2011a) Fungal gene expression on demand: an inducible, tunable, and metabolism-independent expression system for *Aspergillus niger*. *Appl Environ Microbiol* **77:** 2975–2983.

Meyer, V., Wu, B., and Ram, A.F.J. (2011b) *Aspergillus* as a multi-purpose cell factory: current status and perspectives. *Biotechnol Lett* **33:** 469–476.

Nakayashiki, H., Hanada, S., Quoc, N.B., Kadotani, N., Tosa, Y., and Mayama, S. (2005) RNA silencing as a tool for exploring gene function in ascomycete fungi. *Fungal Genet Biol* **42:** 275–283.

Papagianni, M. (2004) Fungal morphology and metabolite production in submerged mycelial processes. *Biotechnol Adv* **22:** 189–259.

Papagianni, M., and Mattey, M. (2004) Physiological aspects of free and immobilized *Aspergillus niger* cultures producing citric acid under various glucose concentrations. *Process Biochem* **39:** 1963–1970.

Papagianni, M., and Mattey, M. (2006) Morphological development of *Aspergillus niger* in submerged citric acid fermentation as a function of the spore inoculum level. Application of neural network and cluster analysis for characterization of mycelial morphology. *Microb Cell Fact* **5:** 3.

Saudohar, M., Bencina, M., van de Vondervoort, P.J., Panneman, H., Legisa, M., Visser, J., and Ruijter, G.J. (2002) Cyclic AMP-dependent protein kinase is involved in morphogenesis of *Aspergillus niger*. *Microbiology* **148:** 2635–2645.

Schape, P., Kwon, M.J., Baumann, B., Gutschmann, B., Jung, S., Lenz, S., *et al*. (2019) Updating genome annotation for the microbial cell factory *Aspergillus niger* using gene co-expression networks. *Nucleic Acids Res* **47:** 559–569.

Shannon, P., Markiel, A., Ozier, O., Baliga, N.S., Wang, J.T., Ramage, D., *et al*. (2003) Cytoscape: a software environment for integrated models of biomolecular interaction networks. *Genome Res* **13:** 2498–2504.

Stajich, J.E., Harris, T., Brunk, B.P., Brestelli, J., Fischer, S., Harb, O.S., *et al*. (2012) FungiDB: an integrated functional genomics database for fungi. *Nucleic Acids Res* **40:** D675–D681.

Steiger, M.G., Rassinger, A., Mattanovich, D., and Sauer, M. (2019) Engineering of the citrate exporter protein enables high citric acid production in *Aspergillus niger*. *Metab Eng* **52:** 224–231.

Sun, X., Wu, H., Zhao, G., Li, Z., Wu, X., Liu, H., and Zheng, Z. (2018) Morphological regulation of *Aspergillus niger* to improve citric acid production by *chsC* gene silencing. *Bioprocess Biosyst Eng* **41:** 1029–1038.

Tong, Z., Zheng, X., Tong, Y., Shi, Y.C., and Sun, J. (2019) Systems metabolic engineering for citric acid production by *Aspergillus niger* in the post-genomic era. *Microb Cell Fact* **18:** 28.

Urita, A., Ishibashi, Y., Kawaguchi, R., Yanase, Y., and Tani, M. (2021) Crosstalk between protein kinase A and the HOG pathway under impaired biosynthesis of complex sphingolipids in budding yeast. *FEBS J* **289:** 766–786.

Wanka, F., Cairns, T., Boecker, S., Berens, C., Happel, A., Zheng, X., *et al*. (2016) Tet-on, or Tet-off, that is the question: advanced conditional gene expression in *Aspergillus*. *Fungal Genet Biol* **89:** 72–83.

Wucherpfennig, T., Hestler, T., and Krull, R. (2011) Morphology engineering–osmolality and its effect on Aspergillus niger morphology and productivity. *Microb Cell Fact* **10:** 58.

Xie, S., Shen, B., Zhang, C., Huang, X., and Zhang, Y. (2014) sgRNAcas9: a software package for designing CRISPR sgRNA and evaluating potential off-target cleavage sites. *PLoS One* **9:** e100448.

Zhang, L., Zheng, X., Cairns, T.C., Zhang, Z., Wang, D., Zheng, P., and Sun, J. (2020) Disruption or reduced expression of the orotidine-5'-decarboxylase gene *pyrG* increases citric acid production: a new discovery during recyclable genome editing in *Aspergillus niger*. *Microb Cell Fact* **19:** 76.

Zheng, X., Yu, J., Cairns, T.C., Zhang, L., Zhang, Z., Zhang, Q., *et al.* (2019a) Comprehensive improvement of sample preparation methodologies facilitates dynamic metabolomics of *Aspergillus niger*. *Biotechnol J* **14:** e1800315.

Zheng, X., Zheng, P., Zhang, K., Cairns, T.C., Meyer, V., Sun, J., and Ma, Y. (2019b) 5S rRNA promoter for guide RNA expression enabled highly efficient CRISPR/Cas9 genome editing in *Aspergillus niger*. *ACS Synth Biol* **8:** 1568–1574.

Zhou, Z., Du, G., Hua, Z., Zhou, J., and Chen, J. (2011) Optimization of fumaric acid production by *Rhizopus delemar* based on the morphology formation. *Bioresour Technol* **102:** 9345–9349.

Znidarsic, P., Komel, R., and Pavko, A. (2000) Influence of some environmental factors on *Rhizopus nigricans* submerged growth in the form of pellets. *World J Microb Biotechnol* **16:** 589–593.

Supporting information

Additional supporting information may be found online in the Supporting Information section at the end of the article.

Fig. S1 Gene disruption and titratable expression of *pkaC* constructed by 5S rRNA-based CRISPR/Cas9 system in *A. niger*.

Fig. S2 *pkaC* conditional mutant resulted in the abnormal conidiophore.

Fig. S3 Conidia morphological characteristics of *pkaC* conditional expression mutants.

Fig. S4 Module membership (MM) and gene significance (GS) of pellet solidity (A) and MN value (B) in the turquoise module.

Fig. S5 Predicted regulation network of PkaC based on the coexpression analysis.

Fig. S6 Gene expression profiling of chitin syntheses involved in cell wall biosynthesis in *pkaC* conditional expression mutants.

Table S1 *A. niger* strains used in the study.

Table S2 Protospacers used in this study.

Table S3 Plasmids used in this study.

Table S4 Primers used in this study.

Table S5 Summary of RNA sequencing and mapping in this study.

Table S6 Gene expression matrix of all samples of the conditional expression mutant in submerged citric acid fermentation with different concentration of Dox.

Table S7 List of genes in each module based on the WGCNA analysis.

Table S8 Complete list of the functional enrichment analysis for turquoise and blue modules.

Table S9 Complete list of the hub genes in each module.

Table S10 Complete list of the functional enrichment analysis for the hub genes in turquoise and blue modules.

Table S11 Hub regulators in turquoise module with high gene significances for citrate production.

Table S12 Hub regulators in blue module with high gene significances for pellet solidity.

